Performance assessment of an eco-friendly tandem solar cell based on double perovskite $Cs_2AgBiBr_6$

Chrafih, Younes; Al-Hattab, Mohamed; El Boubekri, A.; Rahmani, Khalid; Bajjou, Omar; Basyooni, Mohamed A.

DOI
10.1016/j.jpcs.2023.111815

Publication date
2024

Document Version
Final published version

Published in
Journal of Physics and Chemistry of Solids

Journal of Physics and Chemistry of Solids 187 (2024) 111815

Contents lists available at ScienceDirect

Journal of Physics and Chemistry of Solids

journal homepage: www.elsevier.com/locate/jpcs

Performance assessment of an eco-friendly tandem solar cell based on double perovskite $Cs_2AgBiBr_6$

Younes Chrafih [a,*], Mohamed Al-Hattab [b,**], A. El Boubekri [c], Khalid Rahmani [d], Omar Bajjou [b], Mohamed A. Basyooni M. Kabatas [e,f]

[a] LPHE-Modeling and Simulation, Faculty of Sciences, Mohammed V University in Rabat, Rabat, Morocco
[b] Laboratory of Engineering in Chemistry and Physics of Matter (LICPM), Faculty of Sciences and Technics, Sultan Moulay Slimane University, BP 523, 23000, Beni Mellal, Morocco
[c] LGEM, FST, Sultan Moulay Slimane University, BP 523, 23000, Beni Mellal, Morocco
[d] Ecole Normale Supérieure (ENS), Mohammed V University in Rabat, Morocco
[e] Department of Precision and Microsystems Engineering, Delft University of Technology, Mekelweg 2, 2628 CD, Delft, Netherlands
[f] Department of Nanotechnology and Advanced Materials, Graduate School of Applied and Natural Science, Selçuk University, Konya, 42030, Turkey

ARTICLE INFO

Keywords:
$Cs_2AgBiBr_6$
Tandem solar cell
DFT
Solar cell
Scaps-1d

ABSTRACT

Tandem solar cells have a wider photon absorption range, allowing them to provide better efficiency than single-junction SC. The upper cell absorbs high-energy photons, while the lower cell absorbs low-energy filtered photons. However, in order to obtain affordable, efficient, and long-lasting SC, the absorber layers of the *top* and *bottom* cells must be integrated with an adequate bandgap. This research suggests tandem perovskite solar cells as upper band active materials in this setting. The Si homojunction solar cell's performance was improved by investigating the thicknesses of the $p-type$ and $n-type$ layers, doping concentrations, and defect densities. The thickness variation of the *perovskite* solar cell $(100-400\ nm)$ is then optimized. To precisely replicate the tandem devices, the estimated spectra of the perovskite SC are optically filtered onto the lower cells. Current matching was achieved by adjusting the thickness of the *perovskite* sub-cell with different bottom layer thicknesses, and the optimized efficiency of 36.26% for the *perovskite*/*Si* tandem device was shown. The discoveries will open the door for the upcoming creation of $high-efficiency$, low-energy solar cells.

Author statement

This is our original work. We guarantee that we have not plagiarized others work. The work described has not been submitted elsewhere for publication, in whole or in part, and all the authors listed have approved the manuscript that is enclosed. If accepted, it will not be published elsewhere in the same form, in English or in any other language, without the written consent of the Publisher. If any additional materials required, please feel free to contact us at once.

1. Introduction

The world is moving away from energy conversion methods based on fossil fuels and toward clean, *renewable* energy [1]. Production of SC typically rises twice a year. In order to absorb the sunlight that enters solar cells, a variety of materials are utilized as absorbers. According to the absorber material used, solar cells are divided into generations, with organic solar cells being the third generation [2–4]. Other uses for perovskite include a wide range of industries. The first are pricey solar cells made solely of silicon. Low-cost amorphous *Si* solar cells are the second type. The third generation, which has cheap costs, is also being developed; it is highly PCE stabilized. Quantum Dots in applications including photodetectors, Perovskite Solar Cells, and most recently Liang et al. They created high-performance photodetectors using this discovery after successfully fabricating a number of perovskite films [5]. Formula: $ABX3$ (A = monovalent organic/inorganic cation, B = divalent metal, and $X = anion$ (I, Br, Cl, F)) describes organic-inorganic halide perovskites. Pb toxicity, repeatability, and device stability are still serious issues even when the PCE is higher than 25 % [6,7]. Lead-free double halide perovskites with the formula A2BCX6 have exceptional optoelectronic capabilities that are well-recognized in the field of

* Corresponding author.
** Corresponding author.
E-mail address: y.chrafih@um5r.ac.ma (Y. Chrafih).

https://doi.org/10.1016/j.jpcs.2023.111815
Received 11 September 2023; Received in revised form 29 October 2023; Accepted 26 November 2023
Available online 15 December 2023

Nomenclatures

μ_n (cm^2/Vs)	Electron mobility
μ_p (cm^2/Vs)	Mobility of Hole
N_D (cm^{-3})	*Donors concentration*
N_A (cm^{-3})	*Acceptors concentration*
$V_{e(h)}$ (cm/s)	Thermal velocity for electron/Hole
N_c (cm^{-3})	CB effective density of states
N_v (cm^{-3})	VB effective density of states
V_{oc}(V)	*Open circuit voltage*
Q_e(%)	Quantum efficiency
$E_g(eV)$	Band gap energy
χ(eV)	Electron affinity
ε_r	Dielectric permitivity
$Cs_2AgBiBr_6$	Double perovskites
ZnSe	Zinc selenide
ITO	Indium Tin Oxide
Mo	Molybdenum
PV	Photovoltaïque
SC	Solar cell
FF(%)	*Fill Factor*
PCE(η(%))	*Power Conversion Efficiency*
SC	Solar cell
2-T	Two Terminals

photovoltaics [8,9]. They can be thought of as a potential replacement for Pb-based *perovskites* due to their exceptional environmental stability, appealing optoelectronic properties, and low toxicity [10,11]. The development of undesired phases makes HDP (halide double perovskites) synthesis difficult. Recently produced compounds include Cs_2NaBiI_6 [12], $Cs_2AgInCl_6$ [13,14], $Cs_2AgSbCl_6$ [15], and Cs_2AgBiX_6 (X = Br, Cl) [16,17]. $Cs_2AgBiBr_6$ is a good prospective replacement for Pb-based perovskites because of its nontoxicity and remarkable properties appropriate for PSCs. However, the $Cs_2AgBiBr_6$ HDPs still exhibit significant limitations, including a broad interdite indirect band, a strong *electron* − *phonon* couplage, and dominant surface defects [11]. Greul et al. already built the device configuration FTO/c-TiO_2/m--TiO_2/$Cs_2AgBiBr_6$/spiro-OMeTAD/Auutilizing the solution process approach, with a *PCE* of 2.43% [18]. An antisolvent solution procedure was previously used to construct a $Cs_2AgBiBr_6$-based SC with a PCE of 1.26 % (*FTO*/c-TiO_2/m TiO_2/$Cs_2AgBiBr_6$/ *PTAA*/*Au*) [19]. Furthermore, a $Cs_2AgBiBr_6$-based SC (*ITO*/ *SnO*$_2$/Cs_2AgBr_6/ *P3HT*/ *Au*) with 1.44 % efficiency was developed using the low-pressure aided solution approach [20]. *Zhao et al.* developed a device based on a thin $Cs_2AgBiBr_6$ film with an *ITO*/ *SnO*$_2$/$Cs_2AgBiBr_6$/ *SpiroOMeTAD*/Au structure (average grain size of around 500 *nm*) [21].

Our goal is to model the multijunction device with *perovskite* substrate (both top and bottom cell) while focusing on various difficulties and options [22]. Additionally, a tandem *SC* with a rigid terminal was made available for the first time. Its open-circuit voltage (V_{oc}) was about 1.7 *V*, and its power conversion efficiency was approximately 18% [23]. Additionally, this research endeavor demonstrates an increase in efficiency of over 30 %. The findings are achieved through in-depth analysis, simulation, and computation on a variety of configurations, which can help to improve the results and performance even more. In order to simulate, calibrate, and test tandem combinations of upper and lower perovskite solar cells, the work has been broadened. We also took into account other sociological and environmental issues, thus in order to lessen their impact, we used a lead-free perovskite as the top cell. This design can produce results that are advantageous in terms of both economics and power conversion efficiency [24].

We studied the potential benefits of implementing the material $Cs_2AgBiBr_6$ as an absorber in tandem SC to improve energy conversion efficiency in this paper. To that purpose, DFT calculations were utilized to explore the electrical and optical properties of $Cs_2AgBiBr_6$ [25], and the SCAPS software was also used to do numerical simulations of the material's application in SCs. The approach and computational specifics are described in the first section. The second section, which similarly summarizes and discusses our findings, goes into detail on the application of the researched material in solar cells.

In this situation, we established a novel device with an ITO/ZnSe/$Cs_2AgBiBr_6$ structure that made use of several ETM/HTM. We improved both their doping densities and thicknesses, and we looked into the effects of the thickness of the absorber, its flaws, and the time and resources needed. Some of the input factors that we examined in terms of how they affected the performance of our device included the defect density at the *HTL*/$Cs_2AgBiBr_6$ and $Cs_2AgBiBr_6$/ *ETL* interfaces, the electrical affinity of the *ETL*, and the work function of the front/back contact.

2. Device design and numerical simulation

2.1. Simulations and the suggested device's architecture

In the present study, the numerical solution is carried out utilizing the *SCAPS* − 1*D* simulation tool [26–29]. The Ghent University developed SCAPS, which simulates photovoltaic devices by resolving fundamental semiconductor equations like the Poison equation and the continuity equations for electrons and holes. It is an effective modeling tool that simulates electronics with up to seven separate semiconductor layers, each with a distinct set of interface and ground faults. The top *perovskite* cell (TP) is first simulated, yielding a PCE of approximately 18.61 %. The bottom silicon-based cell (BC) is then simulated, yielding a PCE of 22.77 %. This method of individual simulation is known as a stand-alone configuration. Furthermore, the simulation is run on multiple spectra and absorber layer thicknesses to determine the present matching condition. The architecture of the top and bottom cells of the structure under study are depicted in Fig. 1(a). In order to solve our problem numerically, we employed the following three equations: (1) *Poisson's equation*, (2)/(3) continuity equations for *electrons*/*holes*, and power conversion efficiency (*PCE*) [30,31] are used to calculate performance indicators such as *FF*, J_{sc}, V_{oc}, and *PCE*..

$$-\frac{d}{dx}\left(\varepsilon(x)\frac{d\psi}{dx}\right)=q\left[p(x)-n(x)+N_d^+(x)-N_a^-(x)\right] \quad (1)$$

$$\frac{\partial j_n}{\partial x}=q\left(R_n-G+\frac{\partial n}{\partial t}\right) \quad (2)$$

$$\frac{\partial j_p}{\partial x}=q\left(R_n-G+\frac{\partial p}{\partial t}\right) \quad (3)$$

n/p: *Total electron*/*hole density*.

N_d^+/ N_a^-: *Ionized donor*/*acceptor* − *like doping concentration*.

j_n/ j_p: *Electron*/*hole current density*.

R_n/ R_p: *Electron*/*hole recombination rates*..

ψ, ε, G, *and* q: The *electrostatic potential*, *permittivity*, *generation rate*, and *electron charge* respectively.

Table 1 lists all the simulated materials' specific electrical properties. The equivalent circuit is used to create the $J-V$ curve of the tandem solar cell from those of each sub-cell in order to create a clone of the tandem device. We have made the assumption that the tunnel junction is perfect, with no optical or electrical loss occurring between the two subcells.

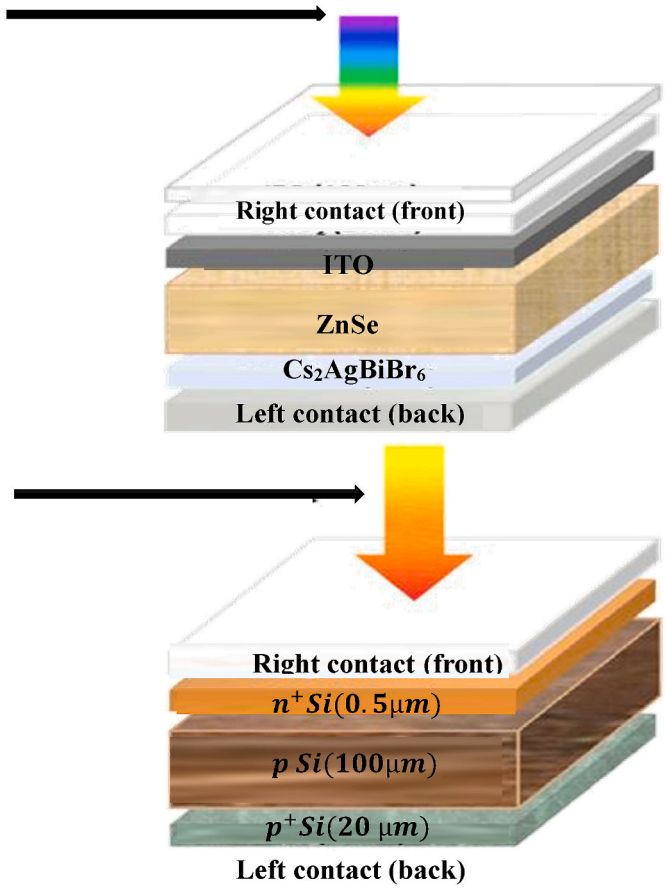

Fig. 1. A cross-sectional illustration of (a) a *BSC* stand-alone bottom cell and (b) an all-perovskite *TSC*, where the typical *AM*1.5 spectrum illuminates the *TC* and the filtered *TC* spectrum is sent to the *BC* for full device simulations.

An optical transmission filter defined by equation (1) is defined on top of the front contact and illuminates the wide bandgap sub-cell with the standard *AM*1.5 *G spectrum*, while the lower narrow bandgap cell is illuminated by a *filtered spectrum* that mimics the optical properties of the *top cell* [32]. Thin-film interference-related reflection losses are not included in this computation. Fig. 1 shows the optical filters made for *perovskite* SC with various band gaps and thicknesses, whereas Fig. 2 shows the absorption coefficients of each layer in *eq*.

Fig. 2 b) depicts the power density of the spectral lines from the 1.5G source, as well as the energy attained by photons entering the cell after passing through different layers of the absorbent $Cs_2AgBiBr_6$ layer. As the absorber's thickness grows, so does its power. According to Fig. 2 b), as the absorber layer with a high band gap thickens, the optical transmission decreases, lowering the Jsc of the lower cellule and limiting the amount of light that can elucidate it. To find the best combination of these characteristics, we investigated how the thickness of the Cs2AgBiBr6 layer affects the photovoltaic properties of two sub-cells. To do this, we used a filtered spectrum calculated with varying absorber film sizes in the upper cellule.

$$S(\lambda) = S_0(\lambda)\left(\exp(\alpha_{ITO}.d_{ITO})\exp(\alpha_{ZnSe}.d_{ZnSe})\exp\left(\alpha_{Cs_2AgBiBr_6}.d_{Cs_2AgBiBr_6}\right)\right) \quad (4)$$

Where:

$\alpha(\lambda)$: *Absorption coefficient*, *d*: *Thickness of a layer*, $S_0(\lambda)$: *AM* 1.5*G spectrum*, $S(\lambda)$: *Filtred spectrum by top cell*,

2.2. Analysis and calibration of a perovskite-based cell (Eg = 1.16 eV) in stand-alone configuration

The aim here is to achieve material savings by reducing the thickness of the $Cs_2AgBiBr_6$ absorber. To achieve this, we carried out a study to optimise the thickness of $Cs_2AgBiBr_6$ while varying its thickness from 0.25 μm to 2 μm. The effect of this adjustment on the suggested solar cell's photovoltaic performance was further researched. First, the upper cell's calibration was performed, and the cell's perovskite thickness was set at 2 μm. The upper cell contained perovskite with a bandgap of 1.417 eV. It can be shown that the two major characteristics of the SC (*PCE* and J_{sc}) grow, then peak at 1.25 μm before declining somewhat for $Cs_2AgBiBr_6$ thickness values between 1.25 μm and 3 μm. It reaches a maximum for the *FF* form factor at a thickness of 1.25 μm and then drops significantly. Based on this result, we may estimate that the optimal thickness of the $Cs_2AgBiBr_6$ absorber is 1.25μm. The open-circuit voltage V_{oc} drops with increasing absorber thickness while remaining high.

The matching $J-V$ and *QE* curves depicted in Fig. 3(a and b) a thorough examination of Fig. 3(a) reveals that raising the perovskite thickness increases the J_{SC} while decreasing cell efficiency. The J_{SC} rises dramatically while the cell V_{oc} stays constant. J_{SC} increases with increasing perovskite thickness because photon absorption increases in the thicker perovskite layer. The rate of electron-hole pair formation rises as a result of the higher cumulative absorption, raising the likelihood of collection and consequently the J_{sc}.

Furthermore, the *top* and *bottom* cells' quantum efficiency [33] is assessed. The quantity of current generated by a solar cell when exposed to photons of a particular wavelength is known as quantum efficiency, which is a crucial solar cell property. Fig. 3 (b) depicts the top and bottom cells' quantum efficiency at varying incoming wavelengths. We found that the highest QE response for the perovskite layer is recorded in the 80–90 % range between 350 and 900 nm, whereas this range is located beyond 1000 nm for Si. This is also visible in Fig. 3 (b), where the

Table 1
Parameters used in the device simulation for every layer.

Parameters	*Materials*					
	Top Cell (*TP*)			*Bottom Cell* (*BC*)		
	ITO	ZnSe	$Cs_2AgBiBr_6$	n^+Si	pSi	p^+Si
Thikness (μm)	0.05	0.08	2	0.5	100	20
Bandgap (*eV*)	3.600	2.900	1.417	1.120	1.120	1.120
Electron Affinity (*eV*)	4.500	4.09	4.190	4.050	4.050	4.050
Dielectric permittivity	8.900	10	5.220	11.900	11.900	11.900
Electron Mobility (cm^2/Vs)	10	50	1.1810	1.400×10^3	1.400×10^3	1.400×10^3
Hole Mobility (cm^2/Vs)	10	20	4.900×10^{-1}	4.500×10^2	4.500×10^2	4.500×10^2
CB effective density of states (cm^{-3})	2.2×10^{18}	1.51×10^{18}	3.25×10^{18}	2.819×10^{19}	2.819×10^{19}	2.819×10^{19}
VB effective density of states (cm^{-3})	1.8×10^{19}	1.81×10^{18}	1.22×10^{19}	1.040×10^{18}	1.040×10^{19}	1.040×10^{19}
N_D (*Doping density* $n-type, 1/cm^3$)	10^{18}	10^{18}	0	10^{15}–10^{19}	0	0
N_A (*Doping density* $p-type, 1/cm^3$)	0	0	8.800×10^{17}	0	1×10^{16}	10^{15}–10^{19}
Electron Thermal Velocity (cm/s)	1×10^7	2.12×10^7	2.381×10^7	1×10^7	1×10^7	1×10^7
Hole Thermal Velocity (cm/s)	1×10^7	1.18×10^7	1.480×10^7	1×10^7	1×10^7	1×10^7

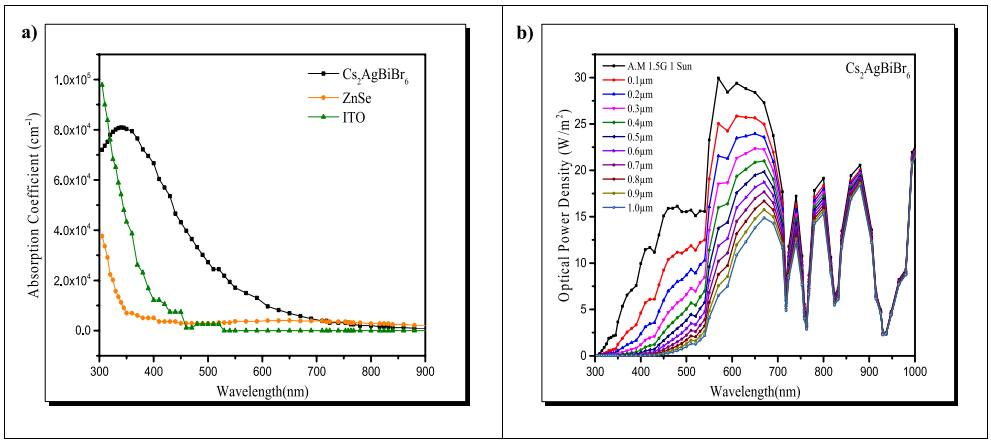

Fig. 2. Absorption coefficient of each ayer in the TSC and the Optical Power Density of the Absorber layer.

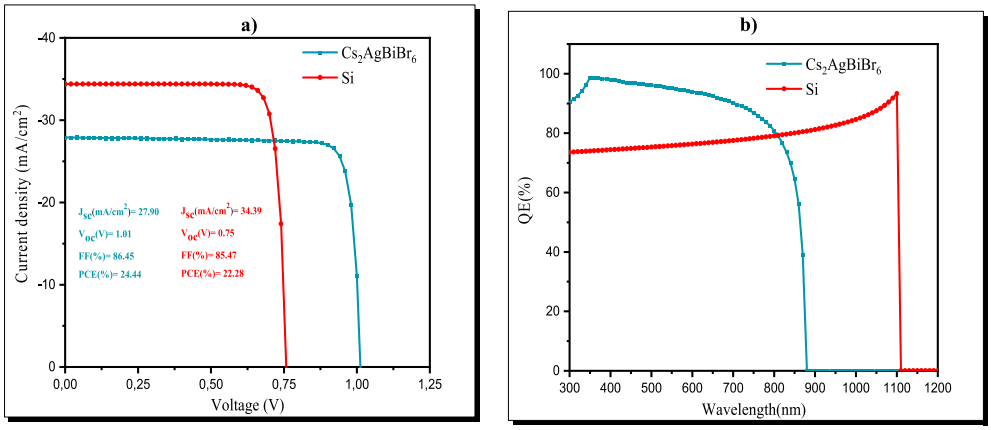

Fig. 3. (a) $J-V$ *curve*, (b) *external QE* for *perovskite* (*top cell*), *Si* (*bottom cell*)..

drop in QE is caused by insufficient light absorption in the thinner perovskite layers. According to the QE diagram of two subcells, the higher cells absorb most of the photon energy at shorter wavelengths. The closeness of the QE between the simulated and experimental operations confirms the simulation design, it should be underlined. After calibration of the sub cells (Top and Bottom) we opted for many values of the most important parameters controlling the solar cells functioning. Table 2 below show a summary of the inputs used for each sub cell in the final stage of the simulation study.

2.3. Effect of charge carrier density and $Cs_2AgBiBr_6$ absorber layer thickness

How to create environmentally friendly solar cells with a high (%) using incredibly thin absorber layers is the problem facing solar energy experts [34]. Optimal cell performance is achieved by adjusting the absorber layer carrier concentration and thickness, which have a considerable impact on the structural design of solar cells. Fig. 4 illustrates how concentration and thickness affect the photovoltaic performance of the proposed solar cell. The concentration and thickness of the $Cs_2AgBiBr_6$-based absorber layer were altered between $10^{13} \rightarrow 10^{18}$ cm^{-3} and 0.2 $\mu m \rightarrow 2$ μm, respectively, in order to investigate the cell's performance. The thickness of the $Cs_2AgBiBr_6$ absorber layer is shown in Fig. 4 to be an essential parameter for cell performance. The efficiency of the cell's energy conversion can be decreased by adjusting the thickness of this layer. V_{oc} increases a little bit as the $Cs_2AgBiBr_6$ absorber layer's thickness and concentration rise. J_{sc} increases from 8.50 → 30.20 mA/cm^2 when absorber layer thickness increases between 0.2 μm and 2 μm, owing to enhanced absorption of longer wavelength photons in this layer, which is similar with the findings of [35,36]. The maximal J_{sc} contour zone does expand into the area of greater thickness, but the concentration of acceptors continues to be largely independent of the absorption layer on the other hand.

As a result, J_{sc} decreased marginally. Due to an increase in the device's series resistance, the form factor (*FF*) drastically dropped as the $Cs_2AgBiBr_6$ thickness grew. The simulated device can have a η(%) > 22 % with a concentration ranging from $10^{16} \rightarrow 10^{18}$cm^{-3} and a thickness >1.45 μm (see Fig. 4). A maximum *PCE* (%) of 22.2% was discovered in this study at a user concentration of 10^{18} cm^{-3} and an absorber layer thickness of 2 μm. An increase in the absorber layer carrier concentration ($Cs_2AgBiBr_6 > 10^{17}$cm^{-3}) has a negative effect on device performance (increase in Auger recombination).

The FF of the SC increased from 88.60 % for the absorber layer cell. This increase can be interpreted as a larger rise in the maximum power output of the solar cell with the *ITO*/ZnSe/$Cs_2AgBiBr_6$ configuration. This increase in maximum power is due to the use of absorber perovskite, which reduces charge carrier recombination losses on the rear side, as seen by the *quantum efficiency* curves (see Fig. 3-b). These

Table 2
The photovoltaic properties of the optimized *perovskite* (*top cell*) solar sell and, *Si* (*bottom cell*) solar sell.

Cell type	$V_{oc}(V)$	$J_{sc}(mA/cm^2)$	*FF* (%)	*PCE* (%)
Si (Optimal condition)	0.75	34.39	85.47	22.28
$Cs_2AgBiBr_6$ (Optimal condition)	1.01	27.90	86.45	24.44

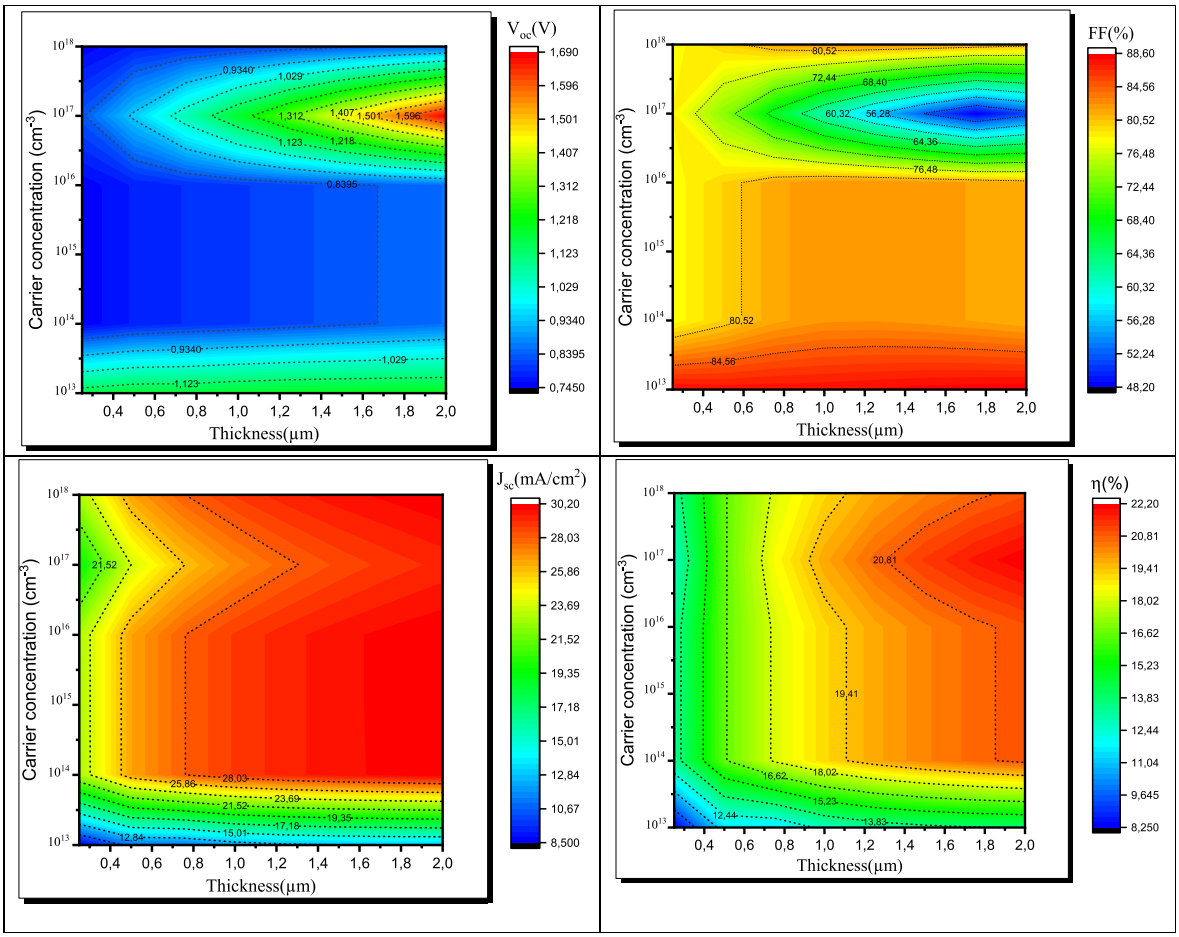

Fig. 4. The contour figure shows how the performance of SC is affected by variation of thickness and carrier concentration of the $Cs_2AgBiBr_6$ absorber layer.

enhancements have led to a notable increase in the *PCE* of the cell, going from 18.06% for the cell without the $Cs_2AgBiBr_6$ layer to 22.20% for the cell with the latter layer inserted due to the stability and good charge carrier generation provided by the latter layer. It should be noted that when the cells are stacked in tandem, the yield improves to approximately 36.26 %.

2.4. $Cs_2AgBiBr_6$/Si tandem solar cell

The top and bottom cells of the tandem device must have an equal current density. The two solar cells in 2 – *T monolithic* tandem devices work as two diodes in series [37]. Thus, the SC that generates the lower current limits the overall current of the tandem device, and the voltage is equal to the sum of the voltages of the upper and lower cells. The bandgap and thickness of the *perovskite* SC were shown to directly affect its J_{sc} in the preceding section. Equation (1) states that when the wide-bandgap absorber layer's thickness increases, optical transmission decreases, lowering the light power impinge on the lower cell and, consequently, the lower cell's J_{sc}. In order to determine the ideal mix of these elements, we investigated the effects of perovskite layer thickness, electron and hole concentrations, and photovoltaic properties of the tandem solar cell. A single filtered transmitted spectrum was produced and utilized to irradiate the lower cell for each top absorber layer thickness that was chosen.

As shown in Fig. 5, for low absorber thicknesses in the higher cell, the current generated diminishes, limiting the tandem device's total J_{SC}. The J_{sc} expands as the perovskite absorber's thickness rises, but it also prevents the top cell's optical transmission, limiting the bottom cell's J_{sc}. As a result, the J_{sc} of the *bottom cell* serves as a limiting factor for the overall J_{sc} once the optimal thickness point is achieved, and the PCE decreases. The optical absorption edge of the *perovskite* layer has a blue shift, which causes the ideal thickness point to change when the bandgap varies. The bandgap and thickness of the perovskite layer, which are 1.417 *eV* and 400 *nm*, respectively, are combined to create the optimal *PCE* of 23.9%. Fig. 5 also illustrates that the J_{sc} is the most important component in tandem device performance and that the V_{oc} and *FF* have little influence on the overall *PCE*. The J_{sc} grows with thickness, as shown in the picture, and the point of intersection between the upper and lower cell curves is the ideal place that establishes the optimal conditions for having a tandem cell with improved features. The point of intersection, as indicated in the picture, implies a current of the order of 24.89 mA/cm^2 with a cell thickness of 400 nm. The bandgap in the higher cell produces a huge V_{oc} of the tandem device, up to almost 1V, as is to be expected. Variations in thickness cause a minor increase in V_{oc}, however the impact of thickness is minimal. The fill factor drops in all bandwidths until it reaches the maximum J_{sc} thickness, at which point a trade-off occurs. Solar cells in tandem commonly exhibit this pattern [38–43].

Fig. 6 shows the simulated current-voltage characteristics of a tandem perovskite/Si solar cell, a bottom filtered Si cell, and an upper perovskite cell with a bandgap of 1.417 *eV* and a thickness of 400 *nm*. As seen in Fig. 6, the *top* and *bottom* cells' short-circuit currents have excellent current matching and are in a similar range. The majority of photon energy is absorbed by the Si sub-cell at long wavelengths, while the perovskite sub-cell mostly does so at short wavelengths, which explains this pattern. Table 3 provides a summary of the photovoltaic characteristics of the simulated 36.26 % tandem solar cell ($Cs_2AgBiBr_6$/c-Si). Table 3 and Fig. 6 show that the bottom sub-cell, whose V_{oc} is

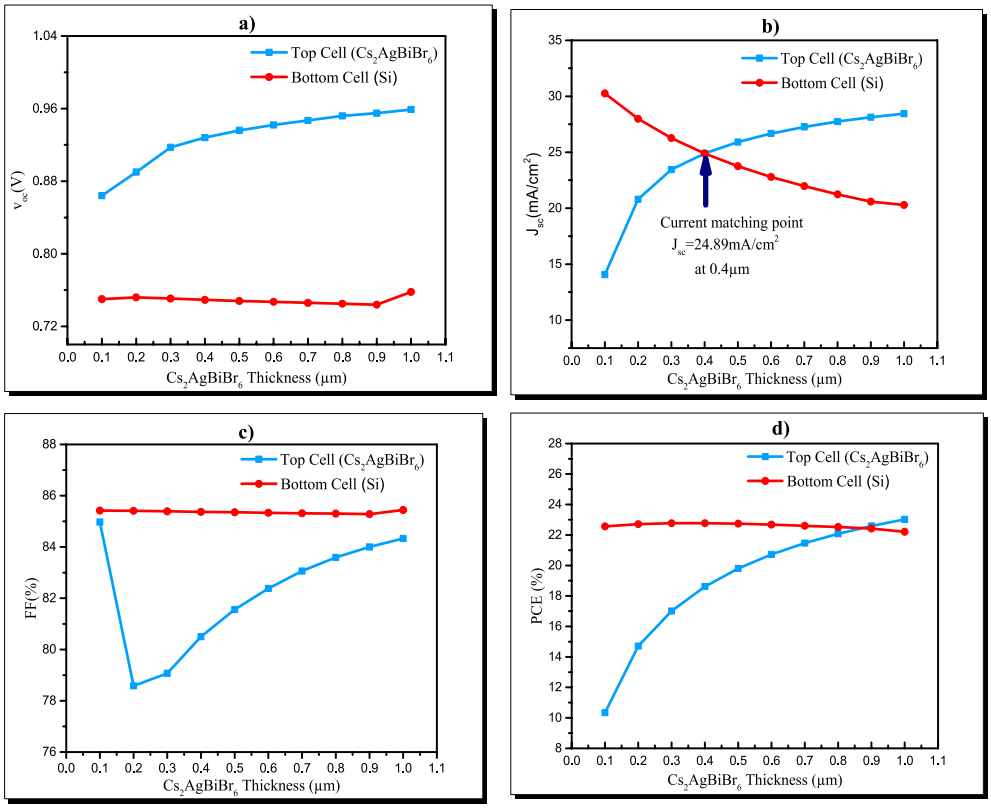

Fig. 5. V_{oc} a), J_{sc} b), *FF* c), and *PCE* d) of the simulated *tandem* SC by variation of thickness of $Cs_2AgBiBr_6$ *perovskite* absorber.

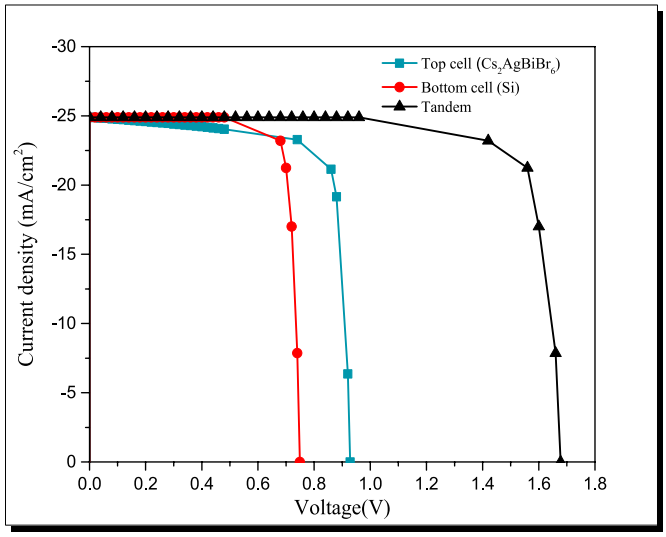

Fig. 6. *J – V curve* for *perovskite* top cell, *Si* bottom cell, and *perovskite/Si tandem* cell.

equal to the sum of the V_{oc} of the two sub-cells, restricts the tandem SC's overall J_{sc}.

Table 4 evaluates the photovoltaic properties of the current work to those of previously published tandem perovskite solar cells. Our findings suggest that it is theoretically conceivable to obtain more than 36 % PCE in *perovskite/homojunction* tandem solar cells; nonetheless, significant challenges remain. Perovskite solar cells have previously attained efficiencies in excess of 25 %, but due to the existing constraints of manufactured Si solar cells, highly efficient perovskite solar cells and highly efficient perovskite/Si tandem devices are not achievable. We demonstrated that by producing highly doped Si layers with a low defect density and a good $p-n$ junction interface (injecting perovskite-based absorber layers), we can improve the performance of Si solar cells.

3. Conclusion

We examined a perovskite/Si tandem solar cell with a PCE of approximately 36.28 % using SCAPS-1D software. Separate numerical simulations of the two solar sub-cells were explored. While the bottom cell first used a spectrum filtered by the top cell, the higher cell was lighted with the *AM* 1.5 *G spectrum*, followed by investigation of the upper perovskites (1.417 *eV*). Then, the absorber layer thickness (20–400 *nm*) and charge carrier density of the two sub-cells were adjusted. In order to match the ideal current, which is achieved by

Table 3
The photovoltaic properties of the optimized *perovskite/Si* tandem SC and its sub-cells are summarized.

Cell type	V_{oc} (*V*)	J_{sc} (*mA/cm*^{2})	*FF* (%)	*PCE* (%)
Si (Optimal condition)	0.75	34.39	85.47	22.28
$Cs_2AgBiBr_6$ (Optimal condition)	1.01	27.90	86.45	24.44
***Top Cell* (400 nm)**	0.928	24.89	80.50	18.61
***Bottom Cell* (*under filtred spectrum*)**	0.7493	24.89	85.37	22.77
Perovskite/Si Tandem Cell	1.6773	24.89	86.87	36.26

Table 4
Results of this study's comparison to real and simulated *perovskite* tandem solar cells.

Device type	$V_{oc}(V)$	$J_{sc}(mA/cm^2)$	*FF* (%)	*PCE* (%)	Reference
Perovskite/Si (Experimental)	1.884	20.26	77.3	29.5	[44]
Perovskite/Si (Experimental)	1.80	18.81	77.5	26.3	[45]
Perovskite/Si (Experimental)	1.68	16.72	75.6	21.2	[46]
Perovskite/Perovskite (Experimental)	2.10	16.80	82.5	29.10	[47]
Perovskite/ Si (Simulation)	1.87	20.3	84.7	32.2	[48]
Perovskite ($Cs_2AgBiBr_6$) (Simulation)	1.20	18.60	50.00	11.35	[49]
Perovskite/ Si (Simulation)	1.76	18.83	73.0	24.2	[50]
Perovskite/ Si (Simulation)	1.80	18.81	77.5	26.3	[51]
Mo/Cs_2AgBiI_6/ZnSe/ITO	50.25	0.54	81.28	22.46	[52]
Mo/$Cs_2AgBiBr_6$/ZnSe/ITO	28.65	1.08	88.44	27.46	[52]
Mo/$Cs_2AgBiCl_6$/ZnSe/ITO	16.56	1.52	90.74	22.85	[52]
Perovskite/ Si (Simulation)	1.6773	24.89	86.87	36.26	**Present work**

conducting current matching for various absorber layer values in the top sub-cell, the two sub-cells were also connected to create a suggested tandem device. Tandem solar cells performed best with an absorber bandgap of 1.417 *eV* and a thickness of 400 *nm*, resulting in a *PCE* of 36.28% and a current density of 24.89 mA/cm^2. We found that the bandgap can be better controlled by employing perovskite in the top cell, which is essential for increasing solar cell efficiency. We believe that by clarifying the effects of perovskite thickness and charge density on cell performance, this study contributes to the body of knowledge on all-perovskite tandem solar cells. Future research and development of highly effective and reasonably priced tandem devices might be guided by the suggested design and optimization strategy.

4. Data accessibility declaration

Data will be provided upon request.

Statement of financial interests

The authors state that they have no conflicts of interest.

Declaration of competing interest

The authors declare that they have no known competing financial interests or personal relationships that could have appeared to influence the work reported in this paper.

Data availability

No data was used for the research described in the article.

Acknowledgments

The computer resources were given by the Laboratory of Modelling and Simulation LPHE-MS, Department of Physics, Mohamed V University, Rabat, which the authors gratefully acknowledge.

The authors also appreciate and thank the Abdus Salam International Centre for Theoretical Physics in Trieste, Italy (with which we have a Federation Scheme) for its cooperation and hospitality.

References

[1] H.L. Tuller, Solar to fuels conversion technologies: a perspective, Mater. Renew. Sustain. Energy 6 (1) (2017) 1–16, https://doi.org/10.1007/s40243-017-0088-2.
[2] M.L. Petrus, J. Schlipf, C. Li, T.P. Gujar, N. Giesbrecht, P. Müller-Buschbaum, M. Thelakkat, T. Bein, S. Hüttner, P. Docampo, Capturing the sun: a review of the challenges and perspectives of perovskite solar cells, Adv. Energy Mater. 7 (16) (2017) 1–27, https://doi.org/10.1002/aenm.201700264.
[3] Xu Chen, Z. Jia, Z. Chen, T. Jiang, L. Bai, F. Tao, J. Chen, Xinya Chen, T. Liu, X. Xu, C. Yang, W. Shen, W.E.I. Sha, H. Zhu, Y. Yang, Michael), Efficient and reproducible monolithic perovskite/organic tandem solar cells with low-loss interconnecting layers, Joule 4 (2020) 1594–1606, https://doi.org/10.1016/j.joule.2020.06.006.
[4] B. Parida, S. Yoon, S.M. Jeong, J.S. Cho, J.K. Kim, D.W. Kang, Recent progress on cesium lead/tin halide-based inorganic perovskites for stable and efficient solar cells: a review, Sol. Energy Mater. Sol. Cells 204 (2020), 110212, https://doi.org/10.1016/j.solmat.2019.110212.
[5] R. Garain, A. Basak, U.P. Singh, Study of thickness and temperature dependence on the performance of SnS based solar cell by SCAPS-1D, Mater. Today Proc. 39 (2021) 1833–1837, https://doi.org/10.1016/j.matpr.2020.06.185.
[6] C. Liang, Hao Gu, J. Xia, T. Liu, S. Mei, N. Zhang, Y. Chen, G. Xing, High-performance flexible perovskite photodetectors based on single-crystal-like two-dimensional Ruddlesden–Popper thin films, Carbon Energy (2022) 1–10, https://doi.org/10.1002/cey2.251.
[7] F. Hao, C.C. Stoumpos, D.H. Cao, R.P. Chang, M.G. Kanatzidis, Nat. Photonics 8 (2014) 489–494.
[8] P.K. Kung, MiH. Li, P.Y. Lin, J.Y. Jhang, M. Pantaler, D.C. Lupascu, G. Grancini, P. Chen, Lead-free double perovskites for perovskite solar cells, Sol. RRL 4 (2) (2020) 1–32, https://doi.org/10.1002/solr.201900306.
[9] A.E. Maughan, A.M. Ganose, D.O. Scanlon, J.R. Neilson, Perspectives and design principles of vacancy-ordered double perovskite halide semiconductors, Chem. Mater. 31 (4) (2019) 1184–1195, https://doi.org/10.1021/acs.chemmater.8b05036.
[10] L.C. Andreani, A. Bozzola, P. Kowalczewski, M. Liscidini, L. Redorici, Silicon solar cells: toward the efficiency limits, Adv. Phys. X 4 (1) (2019), 1548305, https://doi.org/10.1080/23746149.2018.1548305.
[11] Y. Iguchi, K. Inoue, T. Sugiyama, H. Yanagi, Single-crystal growth of Cl-doped n-type SnS using SnCl2 self-flux, Inorg. Chem. 57 (12) (2018) 6769–6772, https://doi.org/10.1021/acs.inorgchem.8b00646.
[12] P. Li, W. Gao, C. Ran, H. Dong, X. Hou, Z. Wu, Post-treatment engineering of vacuum-deposited Cs2NaBiI6 double perovskite film for enhanced photovoltaic performance, Phys. Status Solidi Appl. Mater. Sci. 216 (23) (2019) 1–8, https://doi.org/10.1002/pssa.201900567.
[13] G. Volonakis, A.A. Haghighirad, R.L. Milot, W.H. Sio, M.R. Filip, B. Wenger, M. B. Johnston, L.M. Herz, H.J. Snaith, F. Giustino, Cs2InAgCl6: a new lead-free halide double perovskite with direct band gap, J. Phys. Chem. Lett. 8 (4) (2017) 772–778, https://doi.org/10.1021/acs.jpclett.6b02682.
[14] J. Zhou, Z. Xia, M.S. Molokeev, X. Zhang, D. Peng, Q. Liu, Composition design, optical gap and stability investigations of lead-free halide double perovskite Cs2AgInCl6, J. Mater. Chem. A 5 (29) (2017) 15031–15037, https://doi.org/10.1039/b000000x.
[15] J. Zhou, X. Rong, M.S. Molokeev, X. Zhang, Z. Xia, Exploring the transposition effects on the electronic and optical properties of Cs2AgSbCl6: via a combined computational-experimental approach, J. Mater. Chem. A 6 (5) (2018) 2346–2352, https://doi.org/10.1039/c7ta10062k.
[16] A.H. Slavney, T. Hu, A.M. Lindenberg, H.I. Karunadasa, A Bismuth-Halide double perovskite with long carrier recombination lifetime for photovoltaic applications, J. Am. Chem. Soc. 138 (7) (2016) 2138–2141, https://doi.org/10.1021/jacs.5b13294.
[17] J. Yang, C. Bao, W. Ning, B. Wu, F. Ji, Z. Yan, Y. Tao, J.M. Liu, T.C. Sum, S. Bai, J. Wang, W. Huang, W. Zhang, F. Gao, Stable, high-sensitivity and fast- response photodetectors based on lead-free Cs2AgBiBr6 double perovskite films, Adv. Opt. Mater. 7 (13) (2019), 1801732 https://doi.org/10.1002/.
[18] E. Greul, M.L. Petrus, A. Binek, P. Docampo, T. Bein, Highly stable, phase pure Cs2AgBiBr6 double perovskite thin films for optoelectronic applications, J. Mater. Chem. A 5 (37) (2017) 19972–19981, https://doi.org/10.1039/c7ta06816f.
[19] M. Pantaler, K.T. Cho, V. Queloz, I.G. Benito, C. Fettkenhauer, I. Anusca, M. K. Nazeeruddin, D.C. Lupascu, G. Grancini, Hysteresis-free lead-free double-perovskite solar cells by interface engineering, ACS Energy Lett. 3 (8) (2018) 1781–1786, https://doi.org/10.1021/acsenergylett.8b00871.
[20] C. Wu, Q. Zhang, Y. Liu, W. Luo, X. Guo, Z. Huang, H. Ting, W. Sun, X. Zhong, S. Wei, S. Wang, Z. Chen, L. Xiao, The dawn of lead-free perovskite solar cell: highly stable double perovskite Cs2AgBiBr6 film, Adv. Sci. 5 (3) (2018) 2–9, https://doi.org/10.1002/advs.201700759.
[21] D. Zhao, B. Wang, C. Liang, T. Liu, Q. Wei, S. Wang, K. Wang, Z. Zhang, X. Li, S. Peng, G. Xing, Facile deposition of high-quality Cs2AgBiBr6 films for efficient double perovskite solar cells, Sci. China Mater. 63 (8) (2020) 1518–1525, https://doi.org/10.1007/s40843-020-1346-0.

[22] A. Kumar, M.S. Thomas, G. Pareek, A. Jain, N. Gupta, Performance Evolution of GaAs-Based Solar Cell Towards> 30% Efficiency for Space Applications, 2022, pp. 1–3, https://doi.org/10.1109/5NANO53044.2022.9828955.
[23] L. Benatto, C.F. Marchiori, T. Talka, M. Aramini, N. Yamamoto, S. Huotari, L. Roman, M. Koehler, Thin Solid Films 697 (2020).
[24] E. Meyer, D. Mutukwa, N. Zingwe, R. Taziwa, Metals 8 (2018) 667, https://doi.org/10.3390/met8090667.
[25] Younes Chrafih, Mohamed Al-Hattab, Khalid Rahmani, Thermodynamic, optical, and morphological studies of the Cs2AgBiX6 double perovskites (X = Cl, Br, and I): insights from DFT study, J. Alloys Compd. 960 (2023), 170650, https://doi.org/10.1016/j.jallcom.2023.170650.
[26] K. Chakraborty, M.G. Choudhury, S. Paul, Sol. Energy 194 (2019) 886–892, https://doi.org/10.1016/j.solener.2019.11.005.
[27] A. Basak, U.P. Singh, Sol. Energy Mater. Sol. Cells 230 (2021), https://doi.org/10.1016/j.solmat.2021.111184.
[28] S. Karthick, J. Bouclé, S. Velumani, Sol. Energy 218 (2021) 157–168, https://doi.org/10.1016/j.solener.2021.02.041.
[29] G. Agostinelli, D.L. Bätzner, M. Burgelman, A theoretical model for the front region of cadmium telluride solar cells, Thin Solid Films 431–432 (2003), https://doi.org/10.1016/S0040-6090(03)00263-3, 407–13.
[30] M. Burgelman, P. Nollet, S. Degrave, Modelling polycrystalline semiconductor solar cells, Thin Solid Films 361 (2000) 527–532, https://doi.org/10.1016/S0040-6090(99)00825-1.
[31] I. Alam, M.A. Ashraf, Effect of different device parameters on tin-based perovskite solar cell coupled with In2S3 electron transport layer and CuSCN and Spiro-OMeTAD alternative hole transport layers for high-efficiency performance, Energy Sources, Part A Recover. Util. Environ. Eff. (2020) 1–25, https://doi.org/10.1080/15567036.2020.1820628.
[32] J. Madan, Shivani, R. Pandey, R. Sharma, Device simulation of 17.3% efficient lead-free all-perovskite tandem solar cell, Sol. Energy 197 (2020) 212–221, https://doi.org/10.1016/j.solener.2020.01.006.
[33] L. Wagner, L.E. Mundt, G. Mathiazhagan, M. Mundus, M.C. Schubert, S. Mastroianni, U. Würfel, A. Hinsch, S.W. Glunz, Sci. Rep. 7 (2017) 1–6.
[34] Mohamed Al-Hattab, et al., Numerical simulation of a new heterostructure CIGS/GaSe solar cell system using SCAPS-1D software, Sol. Energy 227 (2021) 13–22.
[35] Bo Li, et al., Efficient and stable Cs2AgBiBr6 double perovskite solar cells through in-situ surface modulation, Chem. Eng. J. 446 (2022), 137144.
[36] Zeyu Zhang, et al., Hydrogenated Cs2AgBiBr6 for significantly improved efficiency of lead-free inorganic double perovskite solar cell, Nat. Commun. 13 (1) (2022) 3397.
[37] J. Burdick, T. Glatfelter, Spectral response and I-V measurements of tandem amorphous-silicon alloy solar cells, Sol. Cell. 18 (3–4) (1986) 301–314, https://doi.org/10.1016/0379-6787(86)90129-8.
[38] A. Nakanishi, Y. Takiguchi, S. Miyajima, Device simulation of CH 3 NH 3 PbI 3 perovskite/heterojunction crystalline silicon monolithic tandem solar cells using an n-type a-Si:H/p-type μc-Si 1–x O x : H tunnel junction, Phys. Status Solidi A 213 (7) (2016) 1997–2002, https://doi.org/10.1002/pssa.201532946.
[39] A. Pathania, R. Pandey, J. Madan, R. Sharma, Design and optimization of 26.3% efficient perovskite/FeSi2 monolithic tandem solar cell, J. Mater. Sci. Mater. Electron. 31 (18) (2020) 15218–15224, https://doi.org/10.1007/s10854-020-04086-z.
[40] R. Pandey, A. Singla, J. Madan, R. Sharma, R. Chaujar, Toward the design of monolithic 23.1% efficient hysteresis and moisture free perovskite/c-Si HJ tandem solar cell: a numerical simulation study, J. Micromech. Microeng. 29 (6) (2019), 064001, https://doi.org/10.1088/1361-6439/ab1512.
[41] Mohamed Al-Hattab, et al., Simulation study of the novel Ag2MgSn(S/Se) 4Chalcogenide tandem solar device employing monolithically integrated (2T) configurations, Sol. Energy 248 (2022) 221–229, https://doi.org/10.1016/j.solener.2022.11.024.
[42] Essaadia Oublal, Mohamed Al-Hattab, Abdelaziz Ait Abdelkadir, Mustapha Sahal, New numerical model for a 2T-tandem solar cell device with narrow band gap SWCNTs reaching efficiency around 35 %, Sol. Energy 246 (2022) 57–65, https://doi.org/10.1016/j.solener.2022.09.036.
[43] Mohamed Al-Hattab, et al., Novel simulation and efficiency enhancement of eco-friendly Cu2FeSnS4/c-Silicon tandem solar device, Silicon 15 (2023) 7311–7319 (October 29, 2023), https://link.springer.com/10.1007/s12633-023-02582-5.
[44] M.A. Green, E.D. Dunlop, J. Hohl-Ebinger, M. Yoshita, N. Kopidakis, X. Hao, C. A. Martin Green, Solar cell efficiency tables (version 59), Prog. Photovoltaics Res. Appl. 30 (2022) 3–12, https://doi.org/10.1002/PIP.3506.
[45] E. Lamanna, F. Matteocci, E. Calabro, L. Serenelli, E. Salza, L. Martini, F. Menchini, M. Izzi, A. Agresti, S. Pescetelli, S. Bellani, A.E. Del Río Castillo, F. Bonaccorso, M. Tucci, A. Di Carlo, Mechanically stacked, two-terminal graphene-based perovskite/silicon tandem solar cell with efficiency over 26, Joule 4 (4) (2020) 865–881, https://doi.org/10.1016/j.joule.2020.01.015.
[46] D. Adachi, J.L. Hernández, K. Yamamoto, Impact of carrier recombination on fill factor for large area heterojunction crystalline silicon solar cell with 25.1% efficiency, Appl. Phys. Lett. 107 (2015), 233506.
[47] M.I. Hossain, M. Shahiduzzaman, A.M. Saleque, M.R. Huqe, W. Qarony, S. Ahmed, M. Akhtaruzzaman, D. Knipp, Y.H. Tsang, T. Taima, Improved nanophotonic front contact design for high-performance perovskite single-junction and perovskite/perovskite tandem solar cell, Sol. RRL 5 (10) (2021), 2100509.
[48] S. Sarker, M.T. Islam, A. Rauf, H. Al Jame, M.R. Jani, S. Ahsan, M.S. Islam, S. S. Nishat, K.M. Shorowordi, S. Ahmed, A SCAPS simulation investigation of non-toxic MAGeI3-on-Si tandem solar device utilizing monolithically integrated (2-T) and mechanically stacked (4-T) configurations, Sol. Energy 225 (2021) 471–485, https://doi.org/10.1016/j.solener.2021.07.057.
[49] M.T. Islam, M.R. Jani, S.M. Al Amin, M.S.U. Sami, K.M. Shorowordi, M.I. Hossain, M. Devgun, S. Chowdhury, S. Banerje, S. Ahmed, Numerical simulation studies of a fully inorganic Cs2AgBiBr6 perovskite solar device, Opt. Mater. 105 (2020), 109957, https://doi.org/10.1016/j.optmat.2020.109957.
[50] K. Yoshikawa, H. Kawasaki, W. Yoshida, T. Irie, K. Konishi, K. Nakano, T. Uto, D. Adachi, M. Kanematsu, H. Uzu, K. Yamamoto, Silicon heterojunction solar cell with interdigitated back contacts for a photoconversion efficiency over 26, Nat. Energy 2 (2017), 17032.
[51] Enrico Lamanna, et al., Mechanically Stacked, Two-Terminal Graphene-Based Perovskite/Silicon Tandem Solar Cell with Efficiency over 26%, vol. 4, 2020, pp. 865–881, https://doi.org/10.1016/j.joule.2020.01.015. Issue 4, 15 April 2020.
[52] Mohamed Al-Hattab, et al., Ab initio investigation for solar technology on the optical and electronic properties of double perovskites Cs2AgBiX 6 (X=Cl, Br, I), ECS Journal of Solid State Science and Technology 12 (9) (2023), 094004, https://doi.org/10.1149/2162-8777/acf7ed.